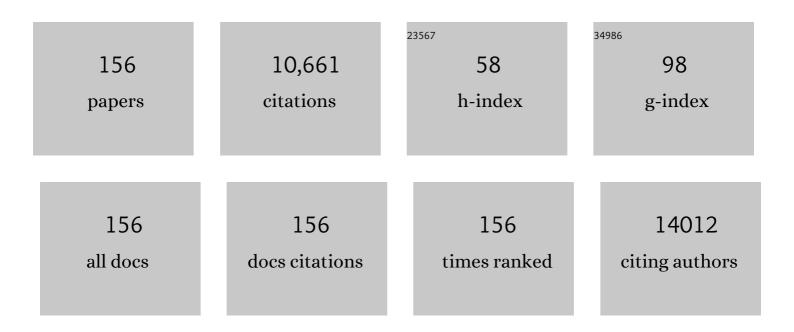
## Xiao Zhang

List of Publications by Year in descending order

Source: https://exaly.com/author-pdf/714907/publications.pdf Version: 2024-02-01



XIAO ZHANC

#	Article	IF	CITATIONS
1	High-Throughput Synthesis of Single-Layer MoS <sub>2</sub> Nanosheets as a Near-Infrared Photothermal-Triggered Drug Delivery for Effective Cancer Therapy. ACS Nano, 2014, 8, 6922-6933.	14.6	813
2	Molecular engineering of dispersed nickel phthalocyanines on carbon nanotubes for selective CO2 reduction. Nature Energy, 2020, 5, 684-692.	39.5	365
3	Product selectivity in plasmonic photocatalysis for carbon dioxide hydrogenation. Nature Communications, 2017, 8, 14542.	12.8	348
4	WS <sub>2</sub> nanosheet as a new photosensitizer carrier for combined photodynamic and photothermal therapy of cancer cells. Nanoscale, 2014, 6, 10394-10403.	5.6	301
5	Functionalized MoS <sub>2</sub> Nanovehicle with Nearâ€Infrared Laserâ€Mediated Nitric Oxide Release and Photothermal Activities for Advanced Bacteriaâ€Infected Wound Therapy. Small, 2018, 14, e1802290.	10.0	259
6	Plasmon-Enhanced Catalysis: Distinguishing Thermal and Nonthermal Effects. Nano Letters, 2018, 18, 1714-1723.	9.1	251
7	Recent Advances in Upconversion Nanoparticlesâ€Based Multifunctional Nanocomposites for Combined Cancer Therapy. Advanced Materials, 2015, 27, 7692-7712.	21.0	243
8	Smart MoS <sub>2</sub> /Fe <sub>3</sub> O <sub>4</sub> Nanotheranostic for Magnetically Targeted Photothermal Therapy Guided by Magnetic Resonance/Photoacoustic Imaging. Theranostics, 2015, 5, 931-945.	10.0	234
9	An Allâ€Organic Semiconductor C <sub>3</sub> N <sub>4</sub> /PDINH Heterostructure with Advanced Antibacterial Photocatalytic Therapy Activity. Advanced Materials, 2019, 31, e1901965.	21.0	215
10	Defectâ€Rich Adhesive Molybdenum Disulfide/rGO Vertical Heterostructures with Enhanced Nanozyme Activity for Smart Bacterial Killing Application. Advanced Materials, 2020, 32, e2005423.	21.0	207
11	Controllable Generation of Nitric Oxide by Nearâ€Infraredâ€Sensitized Upconversion Nanoparticles for Tumor Therapy. Advanced Functional Materials, 2015, 25, 3049-3056.	14.9	194
12	Conductive Graphene Fibers for Wire-Shaped Supercapacitors Strengthened by Unfunctionalized Few-Walled Carbon Nanotubes. ACS Nano, 2015, 9, 1352-1359.	14.6	193
13	Rapid Degradation and High Renal Clearance of Cu <sub>3</sub> BiS <sub>3</sub> Nanodots for Efficient Cancer Diagnosis and Photothermal Therapy <i>in Vivo</i> . ACS Nano, 2016, 10, 4587-4598.	14.6	173
14	TPGS-stabilized NaYbF4:Er upconversion nanoparticles for dual-modal fluorescent/CT imaging and anticancer drug delivery to overcome multi-drug resistance. Biomaterials, 2015, 40, 107-116.	11.4	172
15	One-pot synthesis of PEGylated plasmonic MoO3–x hollow nanospheres for photoacoustic imaging guided chemo-photothermal combinational therapy of cancer. Biomaterials, 2016, 76, 11-24.	11.4	171
16	Poly(Vinylpyrollidone)―and Selenocysteineâ€Modified Bi <sub>2</sub> Se <sub>3</sub> Nanoparticles Enhance Radiotherapy Efficacy in Tumors and Promote Radioprotection in Normal Tissues. Advanced Materials, 2017, 29, 1701268.	21.0	171
17	Efficient Near Infrared Light Triggered Nitric Oxide Release Nanocomposites for Sensitizing Mild Photothermal Therapy. Advanced Science, 2019, 6, 1801122.	11.2	169
18	Electroreduction of CO <sub>2</sub> to Formate on a Copper-Based Electrocatalyst at High Pressures with High Energy Conversion Efficiency. Journal of the American Chemical Society, 2020, 142, 7276-7282.	13.7	165

#	Article	IF	CITATIONS
19	Biodegradable MoO <sub>x</sub> nanoparticles with efficient near-infrared photothermal and photodynamic synergetic cancer therapy at the second biological window. Nanoscale, 2018, 10, 1517-1531.	5.6	144
20	Xâ€Rayâ€Controlled Generation of Peroxynitrite Based on Nanosized LiLuF <sub>4</sub> :Ce <sup>3+</sup> Scintillators and their Applications for Radiosensitization. Advanced Materials, 2018, 30, e1804046.	21.0	138
21	Intelligent MoS <sub>2</sub> Nanotheranostic for Targeted and Enzyme-/pH-/NIR-Responsive Drug Delivery To Overcome Cancer Chemotherapy Resistance Guided by PET Imaging. ACS Applied Materials & Interfaces, 2018, 10, 4271-4284.	8.0	137
22	Oxygen-incorporated MoS2 ultrathin nanosheets grown on graphene for efficient electrochemical hydrogen evolution. Journal of Power Sources, 2015, 291, 195-200.	7.8	133
23	Biodistribution of functionalized multiwall carbon nanotubes in mice. Nuclear Medicine and Biology, 2007, 34, 579-583.	0.6	132
24	Peroxidase-like activity of MoS <sub>2</sub> nanoflakes with different modifications and their application for H <sub>2</sub> O <sub>2</sub> and glucose detection. Journal of Materials Chemistry B, 2018, 6, 487-498.	5.8	130
25	Rhodium Nanoparticles for Ultraviolet Plasmonics. Nano Letters, 2015, 15, 1095-1100.	9.1	119
26	Selective and High Current CO <sub>2</sub> Electro-Reduction to Multicarbon Products in Near-Neutral KCl Electrolytes. Journal of the American Chemical Society, 2021, 143, 3245-3255.	13.7	108
27	Iron Doped CuSn(OH) <sub>6</sub> Microspheres as a Peroxidase-Mimicking Artificial Enzyme for H <sub>2</sub> O <sub>2</sub> Colorimetric Detection. ACS Sustainable Chemistry and Engineering, 2018, 6, 14383-14393.	6.7	103
28	Boosting the lithium storage performance of MoS <sub>2</sub> with graphene quantum dots. Journal of Materials Chemistry A, 2016, 4, 4783-4789.	10.3	100
29	Mesoporous NaYbF4@NaGdF4 core-shell up-conversion nanoparticles for targeted drug delivery and multimodal imaging. Biomaterials, 2014, 35, 7666-7678.	11.4	94
30	In Situ Growth of NiFe Alloy Nanoparticles Embedded into N-Doped Bamboo-like Carbon Nanotubes as a Bifunctional Electrocatalyst for Zn–Air Batteries. ACS Applied Materials & Interfaces, 2018, 10, 26178-26187.	8.0	94
31	FePt nanoparticles-decorated graphene oxide nanosheets as enhanced peroxidase mimics for sensitive response to H2O2. Materials Science and Engineering C, 2018, 90, 610-620.	7.3	93
32	Stimuli-Responsive Small-on-Large Nanoradiosensitizer for Enhanced Tumor Penetration and Radiotherapy Sensitization. ACS Nano, 2020, 14, 10001-10017.	14.6	93
33	Ultralong life lithium-ion battery anode with superior high-rate capability and excellent cyclic stability from mesoporous Fe2O3@TiO2 core–shell nanorods. Journal of Materials Chemistry A, 2014, 2, 3912.	10.3	91
34	Liposomal Delivery of Mitoxantrone and a Cholesteryl Indoximod Prodrug Provides Effective Chemo-immunotherapy in Multiple Solid Tumors. ACS Nano, 2020, 14, 13343-13366.	14.6	91
35	MoS 2 -graphene hybrid nanosheets constructed 3D architectures with improved electrochemical performance for lithium-ion batteries and hydrogen evolution. Electrochimica Acta, 2016, 189, 224-230.	5.2	89
36	Multifunctional Rb <i><sub>x</sub></i> WO <sub>3</sub> Nanorods for Simultaneous Combined Chemoâ€photothermal Therapy and Photoacoustic/CT Imaging. Small, 2014, 10, 4160-4170.	10.0	86

#	Article	IF	CITATIONS
37	Multifunctional WS <sub>2</sub> @Poly(ethylene imine) Nanoplatforms for Imaging Guided Geneâ€Photothermal Synergistic Therapy of Cancer. Advanced Healthcare Materials, 2016, 5, 2776-2787.	7.6	86
38	Self-template synthesis of hierarchical CoMoS <sub>3</sub> nanotubes constructed of ultrathin nanosheets for robust water electrolysis. Journal of Materials Chemistry A, 2017, 5, 11309-11315.	10.3	86
39	Light-Induced Thermal Gradients in Ruthenium Catalysts Significantly Enhance Ammonia Production. Nano Letters, 2019, 19, 1706-1711.	9.1	86
40	A new near infrared photosensitizing nanoplatform containing blue-emitting up-conversion nanoparticles and hypocrellin A for photodynamic therapy of cancer cells. Nanoscale, 2013, 5, 11910.	5.6	85
41	Monodisperse SnO2 anchored reduced graphene oxide nanocomposites as negative electrode with high rate capability and long cyclability for lithium-ion batteries. Journal of Power Sources, 2014, 262, 15-22.	7.8	84
42	Lithium-Ion Intercalation Behavior of LiFePO[sub 4] in Aqueous and Nonaqueous Electrolyte Solutions. Journal of the Electrochemical Society, 2008, 155, A144.	2.9	83
43	In situ synthesis of SnO2–Fe2O3@polyaniline and their conversion to SnO2–Fe2O3@C composite as fully reversible anode material for lithium-ion batteries. Journal of Power Sources, 2014, 246, 862-867.	7.8	82
44	A colorimetric sensor of H <sub>2</sub> O <sub>2</sub> based on Co <sub>3</sub> O <sub>4</sub> –montmorillonite nanocomposites with peroxidase activity. New Journal of Chemistry, 2018, 42, 1501-1509.	2.8	79
45	A quasi-solid-state dye-sensitized solar cell based on the stable polymer-grafted nanoparticle composite electrolyte. Journal of Power Sources, 2006, 160, 1451-1455.	7.8	75
46	Engineered design of theranostic upconversion nanoparticles for tri-modal upconversion luminescence/magnetic resonance/X-ray computed tomography imaging and targeted delivery of combined anticancer drugs. Journal of Materials Chemistry B, 2014, 2, 1379.	5.8	75
47	Si Doped CoO Nanorods as Peroxidase Mimics for Colorimetric Sensing of Reduced Glutathione. ACS Sustainable Chemistry and Engineering, 2019, 7, 13989-13998.	6.7	75
48	Engineering a High-Energy-Density and Long Lifespan Aqueous Zinc Battery via Ammonium Vanadium Bronze. ACS Applied Materials & Interfaces, 2019, 11, 20796-20803.	8.0	75
49	Doping MoS2 with Graphene Quantum Dots: Structural and Electrical Engineering towards Enhanced Electrochemical Hydrogen Evolution. Electrochimica Acta, 2016, 211, 603-610.	5.2	72
50	Revealing the hidden performance of metal phthalocyanines for CO2 reduction electrocatalysis by hybridization with carbon nanotubes. Nano Research, 2019, 12, 2330-2334.	10.4	72
51	Graphene-encapsulated cobalt sulfides nanocages with excellent anode performances for lithium ion batteries. Electrochimica Acta, 2015, 167, 32-38.	5.2	71
52	FeNi Cubic Cage@N-Doped Carbon Coupled with N-Doped Graphene toward Efficient Electrochemical Water Oxidation. ACS Sustainable Chemistry and Engineering, 2018, 6, 8266-8273.	6.7	68
53	Synthesis of well-dispersed Fe <sub>3</sub> O <sub>4</sub> nanoparticles loaded on montmorillonite and sensitive colorimetric detection of H <sub>2</sub> O <sub>2</sub> based on its peroxidase-like activity. New Journal of Chemistry, 2018, 42, 9578-9587.	2.8	65
54	Full Solar‧pectrumâ€Driven Antibacterial Therapy over Hierarchical Sn <sub>3</sub> O <sub>4</sub> /PDINH with Enhanced Photocatalytic Activity. Small, 2021, 17, e2102744.	10.0	64

#	Article	IF	CITATIONS
55	Sol-gel synthesis of mesoporous Co3O4 octahedra toward high-performance anodes for lithium-ion batteries. Electrochimica Acta, 2014, 129, 410-415.	5.2	62
56	Size-tunable rhodium nanostructures for wavelength-tunable ultraviolet plasmonics. Nanoscale Horizons, 2016, 1, 75-80.	8.0	62
57	CoFeP hollow cube as advanced electrocatalyst for water oxidation. Inorganic Chemistry Frontiers, 2019, 6, 604-611.	6.0	61
58	Molecular design of coumarin dyes with high efficiency in dye-sensitized solar cells. Journal of Photochemistry and Photobiology A: Chemistry, 2008, 194, 167-172.	3.9	60
59	Silica-coated bismuth sulfide nanorods as multimodal contrast agents for a non-invasive visualization of the gastrointestinal tract. Nanoscale, 2015, 7, 12581-12591.	5.6	60
60	Highly active oxygen evolution integrated with efficient CO <sub>2</sub> to CO electroreduction. Proceedings of the National Academy of Sciences of the United States of America, 2019, 116, 23915-23922.	7.1	58
61	Graphdiyne nanoradioprotector with efficient free radical scavenging ability for mitigating radiation-induced gastrointestinal tract damage. Biomaterials, 2020, 244, 119940.	11.4	58
62	Nd <sup>3+</sup> sensitized dumbbell-like upconversion nanoparticles for photodynamic therapy application. Journal of Materials Chemistry B, 2016, 4, 2776-2784.	5.8	57
63	Glucose-responsive cascaded nanocatalytic reactor with self-modulation of the tumor microenvironment for enhanced chemo-catalytic therapy. Materials Horizons, 2020, 7, 1834-1844.	12.2	56
64	Efficient bifunctional vanadium-doped Ni <sub>3</sub> S <sub>2</sub> nanorod array for overall water splitting. Inorganic Chemistry Frontiers, 2019, 6, 443-450.	6.0	54
65	Vanadium doping over Ni3S2 nanosheet array for improved overall water splitting. Applied Surface Science, 2019, 489, 815-823.	6.1	50
66	Vanadium and nitrogen co-doped CoP nanoleaf array as pH-universal electrocatalyst for efficient hydrogen evolution. Journal of Alloys and Compounds, 2019, 791, 1070-1078.	5.5	50
67	Topochemical transformation of Co( <scp>ii</scp> ) coordination polymers to Co <sub>3</sub> O <sub>4</sub> nanoplates for high-performance lithium storage. Journal of Materials Chemistry A, 2015, 3, 2251-2257.	10.3	49
68	MoS2 nanosheets decorated Ni(OH)2 nanorod array for active overall water splitting. Journal of Alloys and Compounds, 2019, 796, 86-92.	5.5	49
69	One-dimensional mesoporous Fe2O3@TiO2 core–shell nanocomposites: Rational design, synthesis and application as high-performance photocatalyst in visible and UV light region. Applied Surface Science, 2014, 317, 43-48.	6.1	48
70	Translocation, biotransformation-related degradation, and toxicity assessment of polyvinylpyrrolidone-modified 2H-phase nano-MoS <sub>2</sub> . Nanoscale, 2019, 11, 4767-4780.	5.6	47
71	Near infrared light triggered nitric oxide releasing platform based on upconversion nanoparticles for synergistic therapy of cancer stem-like cells. Science Bulletin, 2017, 62, 985-996.	9.0	45
72	Porphyrin functionalized Co(OH) <sub>2</sub> /GO nanocomposites as an excellent peroxidase mimic for colorimetric biosensing. Analyst, The, 2019, 144, 5284-5291.	3.5	45

#	Article	IF	CITATIONS
73	Construction of sandwiched graphene paper@Fe <sub>3</sub> O <sub>4</sub> nanorod array@graphene for large and fast lithium storage with an extended lifespan. Journal of Materials Chemistry A, 2015, 3, 19384-19392.	10.3	44
74	NiMoS <sub>3</sub> Nanorods as pH-Tolerant Electrocatalyst for Efficient Hydrogen Evolution. ACS Sustainable Chemistry and Engineering, 2017, 5, 9006-9013.	6.7	43
75	A two-step gas/liquid strategy for the production of N-doped defect-rich transition metal dichalcogenide nanosheets and their antibacterial applications. Nanoscale, 2020, 12, 8415-8424.	5.6	43
76	Few-Layer Bismuthene for Checkpoint Knockdown Enhanced Cancer Immunotherapy with Rapid Clearance and Sequentially Triggered One-for-All Strategy. ACS Nano, 2020, 14, 15700-15713.	14.6	41
77	Large and stable reversible lithium-ion storages from mesoporous SnO2 nanosheets with ultralong lifespan over 1000 cycles. Journal of Power Sources, 2014, 268, 365-371.	7.8	40
78	Hybrid catalyst of MoS2-CoMo2S4 on graphene for robust electrochemical hydrogen evolution. Fuel, 2016, 184, 559-564.	6.4	40
79	Electrodepositing Pd on NiFe layered double hydroxide for improved water electrolysis. Materials Chemistry Frontiers, 2019, 3, 842-850.	5.9	40
80	Ni-Co-B nanosheets coupled with reduced graphene oxide towards enhanced electrochemical oxygen evolution. Journal of Alloys and Compounds, 2019, 776, 511-518.	5.5	38
81	Monodisperse spindle-like FeWO4 nanoparticles: Controlled hydrothermal synthesis and enhanced optical properties. Journal of Solid State Chemistry, 2012, 196, 550-556.	2.9	37
82	Loading Pt Nanoparticles on Metal–Organic Frameworks for Improved Oxygen Evolution. ACS Sustainable Chemistry and Engineering, 2017, 5, 11577-11583.	6.7	37
83	Role of Electric Field and Reactive Oxygen Species in Enhancing Antibacterial Activity: A Case Study of 3D Cu Foam Electrode with Branched CuO–ZnO NWs. Journal of Physical Chemistry C, 2018, 122, 26454-26463.	3.1	37
84	Enhanced hydrogen evolution of MoS <sub>2</sub> /RGO: vanadium, nitrogen dopants triggered new active sites and expanded interlayer. Inorganic Chemistry Frontiers, 2018, 5, 2092-2099.	6.0	36
85	A simple and efficient synthetic route for preparation of NaYF <sub>4</sub> upconversion nanoparticles by thermo-decomposition of rare-earth oleates. CrystEngComm, 2014, 16, 5650-5661.	2.6	35
86	Metal Phthalocyanine-Derived Single-Atom Catalysts for Selective CO <sub>2</sub> Electroreduction under High Current Densities. ACS Applied Materials & Interfaces, 2020, 12, 33795-33802.	8.0	35
87	Mesoporous Bamboo Charcoal Nanoparticles as a New Nearâ€Infrared Responsive Drug Carrier for Imagingâ€Guided Chemotherapy/Photothermal Synergistic Therapy of Tumor. Advanced Healthcare Materials, 2016, 5, 1627-1637.	7.6	34
88	Cobalt and nickel bimetallic sulfide nanoparticles immobilized on montmorillonite demonstrating peroxidase-like activity for H <sub>2</sub> O <sub>2</sub> detection. New Journal of Chemistry, 2018, 42, 18749-18758.	2.8	34
89	Synthesis of Surfaceâ€Modificationâ€Oriented Nanosized Molybdenum Disulfide with High Peroxidaseâ€Like Catalytic Activity for H <sub>2</sub> O <sub>2</sub> and Cholesterol Detection. Chemistry - A European Journal, 2018, 24, 15868-15878.	3.3	33
90	Bi <sub>2</sub> S <sub>3</sub> –Tween 20 Nanodots Loading PI3K Inhibitor, LY294002, for Mild Photothermal Therapy of LoVo Cells In Vitro and In Vivo. Advanced Healthcare Materials, 2018, 7, e1800830.	7.6	32

#	Article	IF	CITATIONS
91	Nickel iron boride nanosheets on rGO for active electrochemical water oxidation. Journal of Solid State Chemistry, 2018, 265, 135-139.	2.9	31
92	Liquidâ€Phase Exfoliation and Functionalization of MoS <sub>2</sub> Nanosheets for Effective Antibacterial Application. ChemBioChem, 2020, 21, 2373-2380.	2.6	31
93	White light emission from an exciplex based on a phosphine oxide type electron transport compound in a bilayer device structure. RSC Advances, 2013, 3, 21453.	3.6	29
94	Graphene layer encapsulated MoNi4-NiMoO4 for electrocatalytic water splitting. Applied Surface Science, 2020, 504, 144390.	6.1	29
95	Porous Co3O4 nanorods as anode for lithium-ion battery with excellent electrochemical performance. Journal of Solid State Chemistry, 2014, 213, 193-197.	2.9	28
96	PtFe/nitrogen-doped graphene for high-performance electrooxidation of formic acid with composition sensitive electrocatalytic activity. RSC Advances, 2015, 5, 60237-60245.	3.6	28
97	5,10,15,20-Tetrakis(4-carboxylphenyl)porphyrin modified nickel-cobalt layer double hydroxide nanosheets as enhanced photoelectrocatalysts for methanol oxidation under visible-light. Journal of Colloid and Interface Science, 2020, 561, 881-889.	9.4	28
98	Pie-like free-standing paper of graphene paper@Fe 3 O 4 nanorod array@carbon as integrated anode for robust lithium storage. Chemical Engineering Journal, 2017, 309, 272-277.	12.7	27
99	Facile fabrication of a NiO/Ag <sub>3</sub> PO <sub>4</sub> Z-scheme photocatalyst with enhanced visible-light-driven photocatalytic activity. New Journal of Chemistry, 2020, 44, 12806-12814.	2.8	27
100	A comparative theoretical investigation of ruthenium dyes in dye-sensitized solar cells. Journal of Photochemistry and Photobiology A: Chemistry, 2007, 185, 283-288.	3.9	24
101	FePt nanoalloys anchored reduced graphene oxide as high-performance electrocatalysts for formic acid and methanol oxidation. Journal of Alloys and Compounds, 2014, 604, 286-291.	5.5	24
102	Theory-Driven Design of Electrocatalysts for the Two-Electron Oxygen Reduction Reaction Based on Dispersed Metal Phthalocyanines. CCS Chemistry, 2022, 4, 228-236.	7.8	24
103	Self-template synthesis of CoFe <sub>2</sub> O <sub>4</sub> nanotubes for high-performance lithium storage. RSC Advances, 2015, 5, 29837-29841.	3.6	23
104	Layered FeMo4S6 nanosheets with robust lithium storage and electrochemical hydrogen evolution. Materials Letters, 2016, 183, 1-4.	2.6	23
105	Hierarchical Ni(OH) <sub>2</sub> â€MnO <sub>2</sub> Array as Supercapacitor Electrode with High Capacity. Advanced Materials Interfaces, 2019, 6, 1801470.	3.7	23
106	Ni <sub>3</sub> [Fe(CN) <sub>6</sub> ] <sub>2</sub> nanocubes boost the catalytic activity of Pt for electrochemical hydrogen evolution. Inorganic Chemistry Frontiers, 2018, 5, 1683-1689.	6.0	23
107	Oneâ€Pot Templateâ€Free Synthesis of NaYF <sub>4</sub> Upconversion Hollow Nanospheres for Bioimaging and Drug Delivery. Chemistry - an Asian Journal, 2014, 9, 1655-1662.	3.3	22
108	Liquid Polymer Nanocomposites PEGMEâ^'SnO2and PEGMEâ^'TiO2Prepared through Solvothermal Methods. Chemistry of Materials, 2006, 18, 3850-3854.	6.7	21

#	Article	IF	CITATIONS
109	Fast and large lithium storages from CoMoO4 nanorods-graphene composite. Ionics, 2015, 21, 2993-2999.	2.4	21
110	Sacrificial template formation of CoMoO <sub>4</sub> hollow nanostructures constructed by ultrathin nanosheets for robust lithium storage. RSC Advances, 2016, 6, 51710-51715.	3.6	20
111	Aligned Single-Walled Carbon Nanotube Arrays from Rhodium Catalysts with Unexpected Diameter Uniformity Independent of the Catalyst Size and Growth Temperature. Chemistry of Materials, 2016, 28, 870-875.	6.7	20
112	Mass production of poly(ethylene glycol) monooleate-modified core-shell structured upconversion nanoparticles for bio-imaging and photodynamic therapy. Scientific Reports, 2019, 9, 5212.	3.3	20
113	NixCu6â <sup>~2</sup> xSn5 alloys as negative electrode materials for rechargeable lithium batteries. Journal of Power Sources, 2007, 167, 171-177.	7.8	19
114	A quasi-solid-state dye-sensitized solar cell based on porous polymer electrolyte membrane. Journal of Photochemistry and Photobiology A: Chemistry, 2008, 194, 31-36.	3.9	19
115	Ultrasonic-induced synthesis of high surface area colloids CeO2–ZrO2. Journal of Nanoparticle Research, 2009, 11, 737-741.	1.9	19
116	Self-assembled 3D Co3O4-graphene frameworks with high lithium storage performance. Ionics, 2014, 20, 1635-1639.	2.4	19
117	Accelerated identification of high-performance catalysts for low-temperature NH <sub>3</sub> -SCR by machine learning. Journal of Materials Chemistry A, 2021, 9, 23850-23859.	10.3	19
118	Co-Doped Co[sub x]Cu[sub 6â^'x]Sn[sub 5] Alloys as Negative Electrode Materials for Rechargeable Lithium Batteries. Journal of the Electrochemical Society, 2007, 154, A7.	2.9	18
119	Rapid colorimetric sensing of ascorbic acid based on the excellent peroxidase-like activity of Pt deposited on ZnCo <sub>2</sub> O <sub>4</sub> spheres. New Journal of Chemistry, 2020, 44, 12002-12008.	2.8	18
120	Tumorâ€Tropic Adiposeâ€Derived Mesenchymal Stromal Cell Mediated Bi <sub>2</sub> Se <sub>3</sub> Nanoâ€Radiosensitizers Delivery for Targeted Radiotherapy of Nonâ€Small Cell Lung Cancer. Advanced Healthcare Materials, 2022, 11, e2200143.	7.6	18
121	Fe2.25W0.75O4/reduced graphene oxide nanocomposites for novel bifunctional photocatalyst: One-pot synthesis, magnetically recyclable and enhanced photocatalytic property. Journal of Solid State Chemistry, 2013, 205, 171-176.	2.9	17
122	Functional tumor imaging based on inorganic nanomaterials. Science China Chemistry, 2017, 60, 1425-1438.	8.2	17
123	Evaporation-induced self-assembly synthesis of mesoporous FeCo2O4 octahedra with large and fast lithium storage properties. Materials Letters, 2016, 166, 1-4.	2.6	16
124	MoS2@C nanosphere as near infrared / pH dual response platform for chemical photothermal combination treatment. Colloids and Surfaces B: Biointerfaces, 2020, 192, 111054.	5.0	16
125	Heterogeneous Co@CoO composited P, N co-doped carbon nanofibers on carbon cloth as pH-tolerant electrocatalyst for efficient oxygen evolution. Journal of Alloys and Compounds, 2021, 877, 160279.	5.5	16
126	Synergistic effect between sulfur and CoFe alloys embedded in N-doped carbon nanosheets for efficient hydrogen evolution under neutral condition. Chemical Engineering Journal, 2021, 426, 131922.	12.7	16

#	Article	IF	CITATIONS
127	Selective synthesis of large diameter, highly conductive and high density single-walled carbon nanotubes by a thiophene-assisted chemical vapor deposition method on transparent substrates. Nanoscale, 2016, 8, 14156-14162.	5.6	15
128	Protein-directed synthesis of Bi <sub>2</sub> S <sub>3</sub> nanoparticles as an efficient contrast agent for visualizing the gastrointestinal tract. RSC Advances, 2017, 7, 17505-17513.	3.6	15
129	Mesoporous CuO xerogels constructed by nanorods for high-performance lithium storage. Materials Letters, 2014, 118, 142-145.	2.6	12
130	Ultrafine cobalt–ruthenium alloy on nitrogen and phosphorus co-doped graphene for electrocatalytic water splitting. Journal of the Taiwan Institute of Chemical Engineers, 2019, 104, 75-81.	5.3	12
131	Mesoporous CoFe <sub>2</sub> O <sub>4</sub> octahedra with high-capacity and long-life lithium storage properties. RSC Advances, 2016, 6, 18-22.	3.6	11
132	Ruthenium doped Ni2P nanosheet arrays for active hydrogen evolution in neutral and alkaline water. Sustainable Energy and Fuels, 2020, 4, 1883-1890.	4.9	11
133	Template-free solvothermal synthesis of monodisperse porous LiFePO4 microsphere as a high-power cathode material for lithium-ion batteries. Materials Letters, 2013, 106, 290-293.	2.6	10
134	Tungsten doping magnetic iron oxide and their enhanced lithium ion storage properties. Materials Letters, 2013, 106, 304-307.	2.6	10
135	Understanding the discrepancy between the quality and yield in the synthesis of carbon nanotubes. Nano Research, 2015, 8, 296-302.	10.4	10
136	Organic–Inorganic Composite Nanorods as an Excellent Mimicking Peroxidases for Colorimetric Detection and Evaluation of Antioxidant. ACS Applied Bio Materials, 2020, 3, 2499-2506.	4.6	10
137	Cerium and nitrogen doped CoP nanorod arrays for hydrogen evolution in all pH conditions. Sustainable Energy and Fuels, 2019, 3, 3344-3351.	4.9	9
138	Electrodeposition of Co4S3 on NiCo LDH nanosheet arrays for advanced hydrogen evolution. Materials Letters, 2021, 285, 129057.	2.6	9
139	The Different Bio-Effects of Functionalized Multi-Walled Carbon Nanotubes on tetrahymena pyriformis. Current Nanoscience, 2008, 4, 240-245.	1.2	8
140	Interlayer-expanded VMo2S4 nanosheets on RGO for high and fast lithium and sodium storage. Journal of Alloys and Compounds, 2019, 772, 178-185.	5.5	8
141	Porphyrin-Modified Cobalt Sulfide as a Developed Noble Metal-free Photoelectrocatalyst toward Methanol Oxidation under Visible Light. Journal of Physical Chemistry C, 2020, 124, 26678-26687.	3.1	8
142	Carbon entrapped nanosized Fe3O4 on Ni foam as integrated electrode with large and fast lithium storage. Materials Letters, 2015, 157, 63-66.	2.6	6
143	3D architecture constructed by 2D SnS2-graphene hybrids towards large and fast lithium storage. Materials Letters, 2016, 185, 311-314.	2.6	6
144	Efficient hydrogen evolution by reconstruction of NiMoO <sub>4</sub> –CoO <i>via</i> Mo recombination. Inorganic Chemistry Frontiers, 0, , .	6.0	6

#	Article	IF	CITATIONS
145	One-pot synthesis of ferromagnetic Fe2.25W0.75O4 nanoparticles as a magnetically recyclable photocatalyst. Journal of Nanoparticle Research, 2012, 14, 1.	1.9	5
146	Synthesis of 1D porous Fe 2 O 3 nanostructures using SiO 2 scaffold towards good lithium storages. Materials Letters, 2016, 171, 125-128.	2.6	5
147	Graphoepitaxial effect in the guided growth of SWNT arrays on quartz. Journal of Materials Chemistry C, 2015, 3, 9678-9683.	5.5	4
148	Fabrication of Cu 3 V 2 O 7 (OH) 2 ·2H 2 O nanoplates constructed flowers using Cu 2 O cube as sacrificial template for good lithium storage. Materials Letters, 2017, 188, 291-295.	2.6	4
149	Diameter dependent doping in horizontally aligned high-density N-doped SWNT arrays. Nano Research, 2019, 12, 1845-1850.	10.4	4
150	Self-template synthesis of magnetic cobalt nanotube based on Kirkendall effect. Materials Letters, 2015, 141, 288-290.	2.6	3
151	Effect of interlayer spacing on sodium ion insertion in nanostructured titanium hydrogeno phosphates/carbon nanotube composites. RSC Advances, 2016, 6, 60015-60021.	3.6	3
152	Non-Thermal Plasma-Modified Ru-Sn-Ti Catalyst for Chlorinated Volatile Organic Compound Degradation. Catalysts, 2020, 10, 1456.	3.5	3
153	Coupled Co and Ir nanocrystals on graphite as pH-wide and efficient electrocatalyst for hydrogen evolution. Surfaces and Interfaces, 2021, 24, 101049.	3.0	3
154	Combination of chemotherapy and photothermal methods for in vitro ablation of MCF-7 cancer cells using crinkly core–shell structure MoS2/C@SiO2 nanospheres. Advanced Powder Technology, 2022, 33, 103388.	4.1	3
155	The photothermal and adsorption properties of different surfactant-modified caesium tungsten bronze. Materials Technology, 2020, , 1-11.	3.0	2
156	Quantum study on photophysical and photochemical process of a new photosensitizer: hypomycin B. Journal of Photochemistry and Photobiology A: Chemistry, 2005, 170, 37-43.	3.9	1